https://iopscience.iop.org/article/10.1088/0957-4484/23/1/015708

Nickel-assisted growth and selective doping of $LiGa_5O_8$ nanocrystals in germano-silicate glasses for infrared broadband light-emission

VN Sigaev[1], NV Golubev[1], ES Ignat'eva[1], VI Savinkov[1], R Lorenzi[2], F Meinardi[2], M Campione[2], A Paleari[1,2]

[1]International Laboratory of Glass-based Functional Materials, Mendeleev University of Chemical Technology of Russia, Miusskaya Square 9,125190 Moscow, Russia

[2]Department of Materials Science, University of Milano-Bicocca, Via R. Cozzi 53,I-20125 Milano, Italy

E-mail: alberto.paleari@unimib.it

Abstract. The target of taking advantage of the near-infrared light emission properties of nickel ions in crystals for the design of novel broadband optical amplifiers requires the identification of suitable nanostructured glasses able to embed Ni-doped nanocrystals and to preserve the workability of a glass. Here we show that Ni-doping of Li_2O-Na_2O-Ga_2O_3-GeO_2-SiO_2 glass (with composition 7.5:2.5:20:35:35 and melting temperature 1480 °C, sensibly lower than in Ge-free silicates) enables the selective embedding of nickel ions in thermally grown $LiGa_5O_8$ nanocrystals. The analysis of transmission electron microscopy and X-ray diffraction data as a function of Ni-content (from 0.01 to 1 mol%) indicates that Ni ions promote the nanophase crystallization without affecting nanoparticle size (~6 nm) and concentration (~4×10^{18} cm^{-3}). Importantly, as evidenced by optical absorption spectra, all nickel ions enter into the nanophase, with a number of ions per nanocrystal that depends on the nanocrystal concentration and ranges from 1 to 10^2. Photoluminescence data indicate that fast nonradiative decay processes become relevant only at mean ion-ion distance shorter than 1.4 nm, which enables the incorporation of few Ni ions per nanoparticle without too a large worsening of the light-emission efficiency. Indeed, at 0.1 mol% nickel, the room temperature quantum yield is 9%, with an effective bandwidth of 320 nm.

PACS Numbers:

1. Introduction

In the last decade the amount of data pointing out the promising optical features of Ni^{2+}-doped glass ceramics as infrared emitters for new broadband optical amplifiers has been continuously growing [1-9]. These materials combine the peculiar optical properties of Ni^{2+} ions in crystal hosts with the processing advantages of glasses. On the one hand, nickel ions in octahedral coordination inside crystalline environments give rise to a broadband infrared (IR) [10,11] luminescence with interesting quantum efficiency, whereas low light-emission intensity was observed in the rare cases of IR-emitting Ni^{2+} ions in glasses [12,13]. On the other hand, glasses are definitely more advantageous for optical fibre processing and, more generally, for the fabrication of optical devices. An interesting solution is indeed represented by Ni^{2+}-doped glass ceramics, which show near-IR luminescence with emission yield and lifetime values indeed potentially adequate for applications [14] and, importantly, with an effective emission bandwidth of more than 250 nm [1-9], largely wider than in state-of-the-art erbium-based optical amplifiers. Breakthrough result supporting the perspective of a real feasibility of Ni^{2+}-based amplifiers was the identification of glass compositions enabling the homogeneous segregation of crystalline nanophases embedded in the amorphous matrix, suitable for hosting Ni^{2+} ions, as successfully implemented in other rare-earth doped nanostructured glass ceramics [15-18]. Promising glass compositions are based on Ga-containing silicates embedding precipitated spinel nanocrystal. In spinel compounds, Ga^{3+} ions admit both tetrahedral and octahedral coordination and have a stronger tetrahedral site preference than Ni^{2+} ions [19-21]. Therefore, in these phases, Ni^{2+} ions are preferentially confined in the octahedral sites and increase the IR emission intensity of the glass ceramics [4]. Moreover, the tetrahedral coordination of Ga ions turns out to be compatible with networking processes that

give rise to the formation of amorphous silicate structures from melt quenching, whereas the octahedral coordination is crucial for the promotion of the growth of nanocrystals - such as Ga_2O_3 [22-26] or $LiGa_5O_8$ [26-29] - by heat treatment of the glass and the formation of crystalline nanophases with gallium in six-fold coordinated sites. Very recently, some of us have found preliminary indication that Ni-doped $LiGa_5O_8$ nanocrystals may grow also in germanosilicate glass matrix, where a relevant reduction of the melting temperature, by more than 100 °C, may be achieved [31].

Here we report clear-cut evidences that nickel ions play a relevant role in promoting the crystallization of the segregated nanophase - whose volume fraction and nanosize dispersion are instead quite independent of the Ni-content. Importantly, we also show that increasing nickel concentration causes the perturbation of the nanocrystal structure and the consequent formation of a variety of local environments of Ni^{2+} ions that spectrally broadens the IR emission band. Crucial mechanism responsible for this features is the preferential embedding of nickel ions into the nanophase during the process of thermally induced nanostructuring of the Li_2O-Na_2O-Ga_2O_3-GeO_2-SiO_2 glass system. The detailed knowledge of the effects of nickel embedding in the nanostructuring process and in the spectral modifications of the light-emission features enables the use of Ni-doping for tailoring the optical response of the present nanostructured glass, and of similar systems, to technological applications.

2. Experimental procedure

Glasses with molar composition $7.5Li_2O$-$2.5Na_2O$-$20Ga_2O_3$-$35GeO_2$-$35SiO_2$, with the addition of NiO as doping component (0, 0.01, 0.05, 0.1, 0.5, 1 mol%), were obtained by melting process at 1480 °C for 40 min in Pt crucible, starting from reagent grade Ge, Si, and Ga oxides, and Li and Na carbonates. A fraction of the obtained glass samples was then treated at 690 °C for 15 min to induce the crystallization of $LiGa_5O_8$, according to differential-thermal-analysis data carried out on the same system. Glassceramic materials were then ground and polished, obtaining green transparent slabs of about 1 cm^2 and 2 mm thick. Density (3.680 g/cm^3) and refractive index (1.6245 at 633 nm) of the final materials were determined, respectively, through hydrostatic measurements and by means of a prism coupler refractometer (Metricon 2010), with an uncertainty of about 1‰ in both cases. The purity of the Ni-free reference sample as well as Ni-doped materials was verified by energy-dispersive x-ray fluorescence analysis (Bruker Artax 200), confirming the absence of optically active contaminants (specifically chromium and iron ions) down to the detection limit of few ppm.

The nanostructural features of the synthesized materials were analyzed by x-ray diffractometry (XRD, PANalytical X'Pert PRO) and transmission electron microscopy (TEM, FEI Tecnai G2 F20) techniques. XRD patterns of bulk glassceramics with different Ni-doping level were collected using CuKα radiation over a scanning range $2\theta = 15 - 85°$. Phase identification was based on the JCDFS catalog. Several TEM images were collected for the statistical analysis of nanoparticle size distribution, also collecting the electron diffraction pattern for the identification of the nanocrystal phase. High-resolution images were taken to check the nanoparticle single-crystal features.

Optical absorption spectra were collected in the spectral range from 300 to 2000 nm, with a spectral bandpass of 5 nm, using a double beam spectrophotometer (PerkinElmer Lambda 950). Light-emission measurements were performed in the near IR region by exciting at 635 nm with a solid state laser modulated at the frequency of 200 Hz and at 980 nm by means of a tunable Ti-sapphire laser (Coherent MIRA 9000), using a liquid-nitrogen cooled InGaS photomultiplier (Hamamatsu R5S09-73) with a response time of 1 ns to measure the time-resolved decay of the luminescence. The spectral distribution of the emitted light was determined integrating the signal in the full time window between successive pulses. Quantum yield of light emission was measured with continuous laser excitation, using an integrating sphere as light collector and choosing the sample position maximizing the photoluminescence signal. To estimate the ratio between emitted and exciting photons, we compared the spectral distribution of input light intensity and emission band in three configurations - with and without the sample and with the excitation beam collected by the detector with the sample inside the sphere but not exposed to the direct exciting beam - so as to include the effects of self-absorption and indirect excitation [32]. The total optical response of the detection system was then obtained with a calibrated light source.

3. Results and Discussion

3.1. Nanostructuring

Electron microscopy analysis of heat treated materials evidences the thermally activated segregation of $LiGa_5O_8$ inside the glass, with a homogeneous dispersion of nanometer sized nanoparticles with mean dimension less than 10 nm (Figure 1(a)). High resolution images indeed confirm the expected formation of the crystalline $LiGa_5O_8$ phase and show that the nanoparticles possess single-crystal features (Figure 1(b)). It is worth noting that electron diffraction patterns at low magnification suggest different degree of crystallization at different Ni-content, with less defined reflections in the electron diffraction pattern of the undoped sample (Figures 1(c) and (d)). However, statistical sampling of materials with different Ni-doping does not register significant differences of mean size and size-dispersion of the grown nanoparticles, whose distribution is centred in all samples, included undoped material, at around 6 nm with full dispersion about 3.5 nm wide (Figure 1(e)). Therefore, the segregation mechanism giving rise to the nanoparticle formation is essentially activated by a thermal process, without an active intervention of Ni ions. Interestingly, taking in mind this result, the Ni-dependent shape of the diffraction peaks in XRD patterns (Figure 1(f)) indicates, according to the Scherrer equation for spherical particles, that the extent of the crystalline domain increases at increasing nickel content, causing a narrowing of the diffraction peaks. The integrated area of the diffraction peaks, compared with the broad unstructured feature typical of the XRD pattern of a glass, is instead unaffected by the Ni content. As a result, comparing the data from TEM analysis and XRD patterns (Figure 1(g)), the nickel ions appear to play the role of crystallization agent within each segregated nanoparticle, with larger effects at increasing Ni-content. In other words, the higher the Ni content, the larger the crystalline domain in each $LiGa_5O_8$ nanoparticle at fixed average size, suggesting a larger concentration of Ni ions per nanoparticle. This result might involve a preferential localization of Ni ions in the $LiGa_5O_8$ nanophase, as indeed confirmed by the analysis of the optical absorption spectra in the next section.

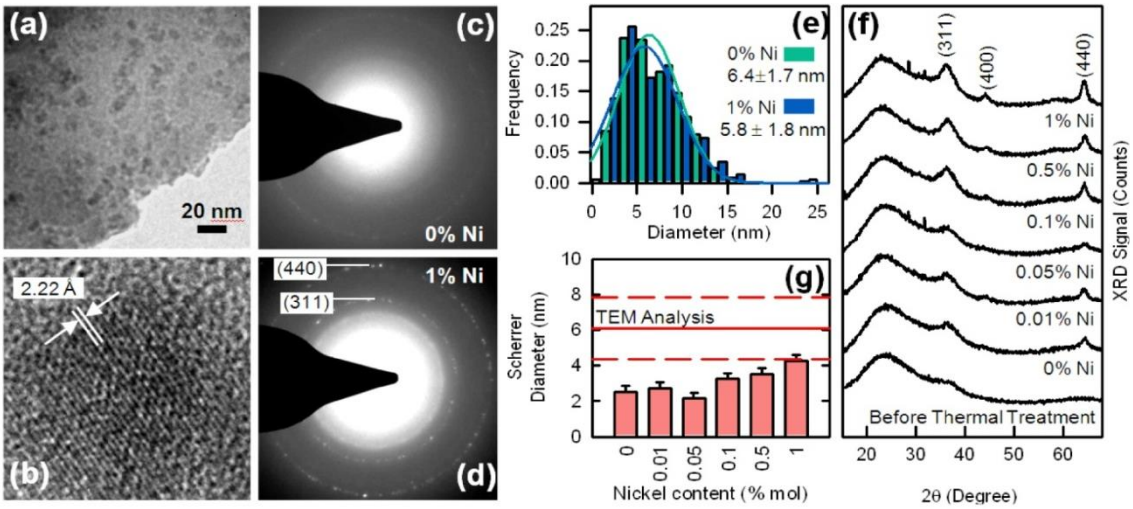

Figure 1. (a) Transmission electron microscopy image of a representative sample of nanostructured $7.5Li_2O$-$2.5Na_2O$-$20Ga_2O_3$-$35GeO_2$-$35SiO_2$ glass, showing the dispersion of segregated nanoparticles. (b) representative high-resolution TEM image of a single nanoparticle evidencing crystalline features corresponding to the $LiGa_5O_8$ lattice parameters. (c) Electron diffraction pattern of undoped nanostructured glassceramics. (d) As (c) but in 1 mol% Ni-doped sample. (e) Nanoparticle size distribution from analysis of TEM images of undoped and 1 mol% Ni-doped nanostructured glassceramics. (f) X-ray diffraction patterns of undoped and Ni-doped nanostructured glassceramics compared with a starting glass sample. (g) Comparison between diameter values of single-crystal domain from Scherrer analysis of XRD data in samples with different Ni-content (bars with uncertainty) and mean value (full line) and standard deviation (dashed lines) obtained from the analysis of TEM images.

3.2. Selective embedding of active ions

Clear-cut confirmation of the selective localization of Ni^{2+} ions into the nanocrystals comes from the Ni-concentration dependence of the optical absorption spectrum of Ni^{2+} ions in octahedral crystalline environment. Comparing the absorption spectrum of Ni^{2+} ions in glassceramics with the spectrum we have found in non-crystallized glass (Figure 2(a)), we note that the characteristic bands at 390, 650, and 1100 nm -

observed in several crystalline materials and corresponding to transitions of Ni^{2+} in octahedral coordination [3,6,9,25,26] - are not accompanied in glassceramics by any trace of the main absorption band of Ni^{2+} in glass that should fall at 435 nm.

The integrated area of the absorption bands (calculated in optical density) in heat treated samples as a function of the Ni content (inset in Figure 2 for the 1.9 eV band), evidences a strict proportionality between the optical absorption from Ni^{2+} ions in the crystalline nanophase and the nominal concentration of nickel introduced in the material, fully consistent with the preferential embedding into the nanoparticles. In order to estimate the fraction of nickel ions in the nanophase, we have analyzed the optical absorption spectra of the glassceramics samples at around 435 nm, corresponding to the peak position of the most intense absorption band of Ni^{2+} ions in glass (Figure 2). We found that possible hidden contributions at this wavelength from glass-like Ni spectrum would amount to not more than few %, so resulting in more than 90 % of Ni^{2+} ions in the crystalline portion of the material. From the integrated intensity and taking into account nickel concentration, material density, and refractive index (neglecting however, in a first approximation, the refractive index dispersion in the considered spectral range), it is so possible to estimate at around 3×10^{-6}, 5×10^{-6} and 16×10^{-6} the oscillator strength of the main Ni^{2+} transitions at 1.1, 1.9 and 3.2 eV, respectively. It is worth noting that the investigated range of Ni-concentration is quite wide, starting from 13.6×10^{18} cm^{-3} (0.01 mol%) and increasing up to 3.5×10^{20} cm^{-3} (1 mol%). This latter value corresponds to almost 10^2 ions per nanoparticle, since the expected upper limit of concentration of $LiGa_5O_8$ nanoparticles (in the case of full segregation, with Ga_2O_3 as limiting reagent and taking the nanoparticle size distribution from the TEM analysis) is estimated to be 4×10^{18} cm^{-3}. Therefore, based on the indication of full embedding into the nanophase coming from the absorption spectra, more than ten Ni^{2+} ions per nanoparticle are expected at Ni-content overcoming approximately 0.1 mol%, while the mean ion-ion distance ranges between 1 and 5 nm. This latter result is important for the control of the excitation diffusion to non-radiative quenching sites.

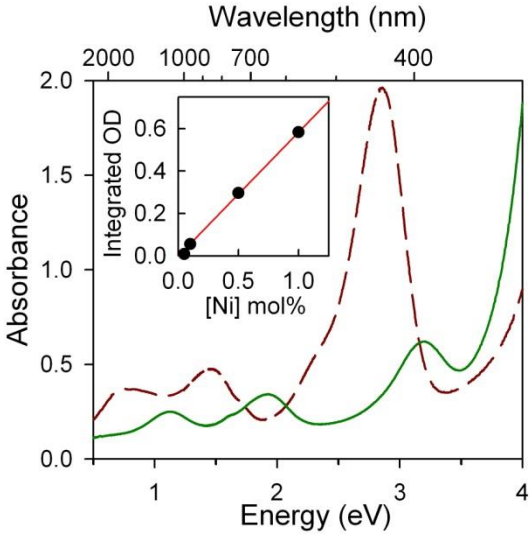

Figure 2. Optical absorption spectra of 0.5 mol% Ni-doped $7.5Li_2O$-$2.5Na_2O$-$20Ga_2O_3$-$35GeO_2$-$35SiO_2$ glass (dashed line) and nanostructured glassceramic (continuous line) samples, about 2 mm thick. Inset: integrated optical density (OD) of the absorption band at about 1.9 eV in nanostructured glassceramics.

3.3. Light-emission features

The selective embedding of Ni^{2+} ions into $LiGa_5O_8$ nanocrystals creates favourable conditions for achieving good light emission properties in the near IR region. Photoluminescence measurements indeed show, as we can see in the representative spectra (collected by exciting at 635 nm) and reported in Figure 3(a), a broad emission band in the near IR spectral region, as expected from Ni^{2+} ions in octahedral coordination [3,6,9,25,26], with the highest amplitude at the concentration of 0.1 mol% of nickel. Excitation at 980 nm gives rise to identical spectra, but with an efficiency about an order of magnitude higher. On the contrary, neither untreated –as quenched and thermal treated- nor undoped samples give rise to any appreciable IR photoluminescence signal. Confirming that IR emission is entirely ascribable to Ni ions located within the nanocrystals, where they experience the appropriate local environment.

Interestingly, the wavelength of the maximum depends on the Ni content, and the band shape shows structured features suggesting at least two spectral components centred approximately at 1300 and 1500 nm (inset of Figure 3(a)). The high-energy component falls at the spectral position expected from Ni^{2+} luminescence in crystals, also observed in nanocrystallized glasses at not too high Ni-doping level, and indeed turns out to be the main contribution at Ni concentration not higher than 0.1 mol%. Instead, the low-energy component becomes more and more relevant in heavy Ni-doped samples, evidencing the increase of a second variant of light-emitting Ni^{2+} sites.

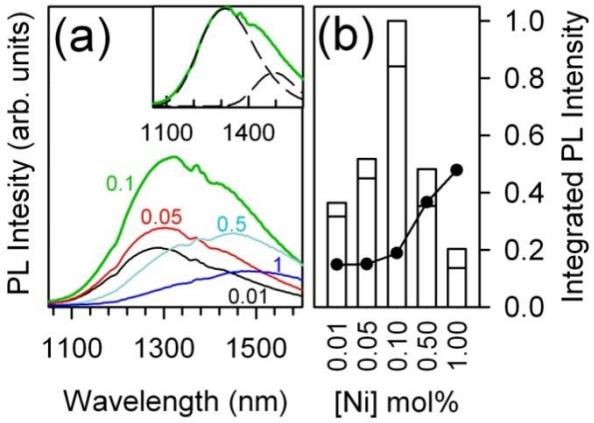

Figure 3. (a) Photoluminescence spectra of Ni^{2+} ions excited at 635 nm in nanostructured $7.5Li_2O$-$2.5Na_2O$-$20Ga_2O_3$-$35GeO_2$-$35SiO_2$ glassceramic at room temperature at different Ni contents; inset: representative two-component Gaussian analysis of PL spectrum in 0.1 mol% Ni-doped sample. (b) Ni-dependence of the integrated photoluminescence spectrum (full bars), normalized at the maximum value observed in 0.1 mol% Ni-doped sample, and integrated intensity of the short- and long-wavelength Gaussian components (lower and higher portions of the bars, respectively), with the ratio of integrated PL intensities (points).

As a result of the overlapping spectral contributions, luminescence ranges over about 300 nm. The observed values of the effective bandwidth, defined as the ratio $[\int I(\lambda)d\lambda)]/I_{max}$ between the integrated emitted intensity and the peak intensity, are reported in Table 1, with the largest bandwidth (326 nm) in the glassceramic sample containing 0.5 mol% of Ni content. The integrated intensity of the luminescence band, as well as the distinct contributions and the ratio of the two components evaluated by Gaussian analysis, are reported in Figure 3(b) as a function of the Ni content. The non-monotonic dependence, with maximum light emission at 0.1 mol%, evidences competitive effects of Ni doping: the increase of light emitting Ni sites and the enhancement of non-radiative decay processes favoured by the increment of nickel concentration. In fact, looking at the luminescence decay kinetics in Figure 4(a), obtained by exciting at 635 nm, we observe that the decay time is progressively shorter at increasing Ni content, with a drastic fastening of the decay rate at nickel concentration higher than 0.1 mol%. The kinetics are not purely single exponential. In order to compare the luminescence decay features in the different samples, we report in Table 1 the effective half-life decay time - defined as the time after which the signal is decreased by a factor 2 - measured at 1400 nm. Only quite minor differences of lifetime, within approximately 20 %, are observed by changing the wavelength within the spectral range of the IR luminescence of each sample, whereas, comparing different samples, the effective decay time changes from more than 0.3 ms at the lowest Ni concentration to only 10 μs at the highest Ni doping, with a drastic lowering at Ni doping above 0.1 mol%.

Table 1. Spectral and kinetic features of the infrared photoluminescence in Ni-doped nanostructured $7.5Li_2O$-$2.5Na_2O$-$20Ga_2O_3$-$35GeO_2$-$35SiO_2$ glassceramic at room temperature

[Ni] mol%	integrated relative intensity	effective bandwidth (nm)	half-life time (μs)
0.01	0.35	290	360

0.05	0.50	302	240
0.1	1.00	318	130
0.5	0.50	326	15
1	0.22	304	10

This result allows us to obtain information on the critical ion-ion distance for the energy transfer - the Förster radius - in order to optimize the system for light-emission and to design specific sets of nanostructuring parameters, including nanoparticle size and concentration. Indeed, we may express the Ni-doping level as number of ions per nanoparticle or, consequently, as mean ion-ion distance R in the nanophase. In this way, the Ni-dependence of the decay time τ_{PL} turns out to follow the behaviour we expect as a result of the increase of the decay rate k_{ET} arising from diffusion towards quenching sites mediated by ion-ion energy transfer (see Figure 4(b)). In fact, since the energy transfer mechanism is favoured by the shortening of the ion-ion distance R down to value comparable to the Förster radius R_0, we expect that $\tau_{PL}(R)$ might be described by the following relation [32],

$$\tau_{PL} = (k_0 + k_{ET})^{-1} \quad \text{with} \quad k_{ET} \propto \left[1 + \left(\frac{R}{R_0}\right)^6\right]^{-1} \tag{1}$$

where k_0 is the decay rate in the limit of null contribution from diffusion to quenching sites mediated by energy transfer processes. Equation (1) indeed accurately describes the experimental data (Figure 4(b)) and enables to estimate around 1.4 nm the value of the Förster radius R_0 in this system. We note that the drastic growth of the low-energy luminescence component (Figure 3(b)) may be related to the increase of the number of nickel ions in the outer shell of the nanoparticle where partially distorted sites may give rise to slightly different luminescence spectral features. Minor substitution of octahedral Li sites [20] by Ni ions may also be a source of structural variants of light-emitting Ni sites.

Importantly, the R_0 value of 1.4 nm gives a chance for enhancing the light-emission yield by increasing the Ni-content at fixed number of Ni ions per nanoparticle, with a suitable design of the glass nanostructuring, so as to avoid too an efficient diffusion of the excitation within each nanoparticle. In the specific set of samples, the nanostructuring and doping features we obtained in the 0.1 mol% Ni-doped material give indeed rise to promising light emission parameters, with about 10 % of quantum yield exciting at 980 nm, with about 320 nm of effective bandwidth centred approximately at 1300 nm.

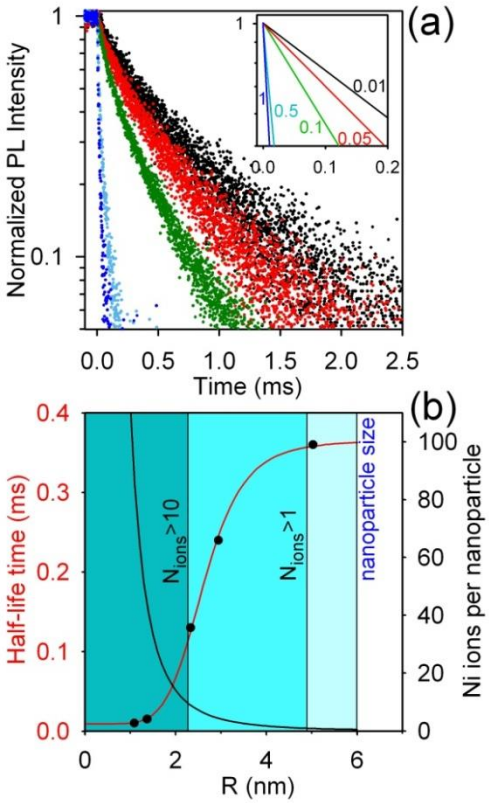

Figure 4. (a) Time decay of the photoluminescence signal (normalized to the starting value) excited at 635 nm at 300 K in nanostructured Ni-doped $7.5Li_2O$-$2.5Na_2O$-$20Ga_2O_3$-$35GeO_2$-$35SiO_2$ glass (the Ni content is indicated in inset in mol% near the lines fitting the first decay step). (b) Half-life time (points) vs mean ion-ion distance R, calculated taking into account full embedding of Ni ions in nanoparticles and data from TEM analysis. The curve through the points is calculated from Equation (1). Right-hand axis indicates the estimated number of Ni ions per nanoparticle according to the curve diverging at small R.

4. Conclusions

The present study allows us to give some insight into the role of Ni ions in the process of crystallization of $LiGa_5O_8$ nanoparticles thermally segregated in the $7.5Li_2O$-$2.5Na_2O$-$20Ga_2O_3$-$35GeO_2$-$35SiO_2$ glass system, and in the resulting light emission properties in the infrared spectral region. Specifically, there are structural and spectroscopic evidences that give clear-cut indication that i) Ni ions act as crystallization agent inside each nanoparticle, but they do not directly activate the $LiGa_5O_8$ nano-segregation; ii) Ni ions are fully embedded in the nanophase at all the investigated doping levels, at least within the experimental uncertainty of the optical absorption measurements; iii) the diffusion of ion excitation promoting the non-radiative decay to quenching sites is regulated by a Förster radius of about 1.4 nm, which enables to embed up to several ions per nanoparticle keeping relatively high light-emission efficiency, up to a quantum yield of about 10 % in the investigated set of samples; iv) about bandwidth, two spectral components, with similar decay properties contribute to the IR luminescence, with Ni-dependent relative intensity.

Importantly, the first two facts assess the possibility of tailoring doping and nanostructuring features of this type of systems without constraints from interactions between Ni ions and nanostructures during synthesis and nanostructructuring process. Specifically, the doping level can be designed to obtain a well defined number of active ions per nanoparticle, whose size and concentration are in turn driven by the gallium content and the parameters of the thermally activated segregation treatment, with negligible perturbation by Ni-doping, at least up to 1 mol%. The other findings suggest specific tools for designing light-emission efficiency and bandwidth by controlling doping and nanostructure features.

Acknowledgments

The authors gratefully acknowledge the financial support for this research by the Ministry of Education and Science of the Russian Federation under Grant No. 11.G34.31.0027, and partially by the Russian Foundation for Basic Research, grant No.09-03-00104.

References

[1] Suzuki T, Horibuchi K and Ohishi Y 2005 Structural and optical properties of ZnO-Al_2O_3-SiO_2 system glass-ceramics containing Ni^{2+}-doped nanocrystals *J.Non-Cryst.Solids* **351** 2304

[2] Zhou S, Dong H, Zeng H, Wu B, Zhu B, Yang H, Xu S, Wan Z and Qiu J 2007 Broadband near-infrared emission from transparent Ni^{2+}-doped silicate glass ceramics *J. Appl. Phys.* **102** 063106

[3] Wu B, Qiu J, Peng M, Ren J, Jiang X and Zhu C 2007 Transparent Ni^{2+}-doped ZnO-Al_2O_3-SiO_2 system glass-ceramics with broadband infrared luminescence *Mater. Res. Bull.* **42** 2007 762

[4] Wu B, Zhou S, Ren J, Qiao Y, Chen D, Zhu C and Qiu J 2008 Enhanced luminescence from transparent Ni^{2+}-doped MgO-Al_2O_3-SiO_2 glass ceramics by Ga_2O_3 addition *J. Phys. Chem. Solids* **69** 891

[5] Feng G, Zhou S, Bao J, Wang X, Xu S and Qiu J 2008 Transparent Ni^{2+}-doped lithium aluminosilicate glass-ceramics with broadband infrared luminescence *J. Alloys Compd.* **457** 506

[6] Wu B, Zhou S, Ruan J, Qiao Y, Chen D, Zhu C and Qiu J 2008 Enhanced broadband near-infrared luminescence from transparent Yb^{3+}/Ni^{2+} codoped silicate glass ceramics *Opt. Express* **16** 1879

[7] Wu B, Ruan J, Qiu J and Zeng H 2009 Enhanced broadband near-infrared luminescence from Ni in Bi/Ni-doped transparent glass ceramics *J. Phys. D: Appl. Phys.* **42** 135110

[8] Deng D, Ma H, Xu S, Wang Q, Huang L, Zhao S, Wang H, Li C 2011 Broadband infrared luminescence of Ni^{2+}-doped silicate glass-ceramics containing lithium aluminate spinel nanocrystals *J. Non-Cryst. Solids* **357** 1426

[9] Zhou S, Jiang N , Wu B, Hao J and Qiu J 2009 Ligand-driven wavelength-tunable and ultra- broadband infrared luminescence in single-ion-doped transparent hybrid materials *Adv. Funct. Mater.* **19** 2081-2088[10] Donegan J F, Bergin F J, Glynn T J, Imbusch G F and Remeika J P 1986 The optical spectroscopy of $LiGa_5O_8$:Ni^{2+} *J. Lumin.* **35** 57

[11] Zannoni E, Cavalli E, Toncelli A, Tonelli M and Bettinelli M 1999 Optical spectroscopy of $Ca_3Sc_2Ge_3O_{12}$:Ni^{2+} *J. Phys. Chem. Solids* **60** 449

[12] Suzuki T and Ohishi Y 2004 Broadband 1400 nm emission from Ni^{2+} in zinc-alumino-silicate glass *Appl. Phys. Lett.* **84** 3804

[13] Gandhi Y, Krishna Mohan N and Veeraiah N 2011 Role of nickel ion coordination on spectroscopic and dielectric properties of ZnF_2-As_2O_3-TeO_2:NiO glass system *J. Non-Cryst. Solids* **357** 1193

[14] Samson B N, Pinckney L R, Wang J, Beall G H and Borrelli N F 2002 Nickel-doped nanocrystalline glass-ceramic fiber *Opt. Lett.* **27** 1309

[15] Driesen K, Tikhomirov V K, Görller-Walrand C, Rodriguez V D and Seddon A B 2006 Transparent Ho^{3+}-doped nano-glass-ceramics for efficient infrared emission *Appl. Phys. Lett.* **88** 073111

[16] Sharonov M Y, Bykov A B, Owen S, Petricevic V, Alfano R R, Beall G H and Borrelli N 2004 Spectroscopic study of transparent forsterite nanocrystalline glass–ceramics doped with chromium *J. Opt. Soc. Am. B* **21** 2046

[17] Velázquez J J, Yanes A C, del Castillo J, Méndez-Ramos J, Rodríguez V D 2007 Optical properties of Ho^{3+}–Yb^{3+} co-doped nanostructured SiO_2–LaF_3 glass-ceramics prepared by sol–gel method *Phys. Status Solidi A-Appl. Mat.* **204** 1762

[18] Brovelli S, Chiodini N, Meinardi F, Monguzzi A, Lauria A, Lorenzi R, Vodopivec B, Mozzati M C and Paleari A 2009 Confined diffusion of erbium excitations in SnO_2 nanoparticles embedded in silica: A time-resolved infrared luminescence study *Phys. Rev. B* **79** 153108

[19] Porta P, Stone F S and Turner R G 1974 The distribution of nickel ions among octahedral and tetrahedral sites in $NiAl_2O_4$-$MgAl_2O_4$ solid solutions *J. Solid State Chem.* **11** 135

[20] Otero Areán C and Trobajo-Fernandez M C 1985 Cation distribution in $Mg_xNi_{1-x}Ga_2O_4$ oxide spinels *Phys. Status Solidi A-Appl. Mat.* **92** 443

[21] Åhman J, Svensson G and Albertsson J 1996 Structure of $LiGa_5O_8$ *Acta Chemica Scandinavica* **50** 391

[22] Zhou S, Dong H, Feng G, Wu B, Zeng H and Qiu J 2007 Broadband optical amplification in silicate glass-ceramic containing β-Ga_2O_3:Ni^{2+} nanocrystals *Opt. Express* **15** 5477

[23] Zhou S, Feng G, Wu B, Jiang N, Xu S and Qiu J 2007 Intense infrared luminescence in transparent glass-ceramics containing β-Ga_2O_3:Ni^{2+} nanocrystals *J. Phys. Chem. C* **111** 7335

[24] Wu B, Zhou S, Ren J, Chen D, Jiang X, Zhu C and Qui J 2007 Broadband infrared luminescence from transparent glass-ceramics containing Ni^{2+}-doped β-Ga_2O_3 nanocrystals *Appl. Phys. B* **87** 697

[25] Xu S, Deng D, Bao R, Ju H, Zhao S, Wang H and Wang B 2008 Ni^{2+}-doped new silicate glass-ceramics for superbroadband optical amplification *J. Opt. Soc. Am. B* **25** 1548

[26] Zhou S, Jiang N, Dong H, Zeng H, Hao J and Qiu J 2008 Size-induced crystal field parameter change and tunable infrared luminescence in Ni^{2+}-doped high-gallium nanocrystals embedded glass ceramics *Nanotechnology* **19** 015702

[27] Suzuki T, Murugan G S and Ohishi Y 2005 Optical properties of transparent Li_2O-Ga_2O_3-SiO_2 glass-ceramics embedding Ni-doped nanocrystals *Appl. Phys. Lett.* **86** 131903

[28] Suzuki T, Arai Y, Ohishi Y 2007 Crystallization processes of Li_2O-Ga_2O_3-SiO_2-NiO system glasses *J. Non-Cryst. Solids* **353** 36

[29] Wu B, Ruan J, Ren J, Chen D, Zhu C, Zhou S and Qiu J 2008 Enhanced broadband near-infrared luminescence in transparent silicate glass ceramics containing Yb^{3+} ions and Ni^{2+}-doped $LiGa_5O_8$ nanocrystals *Appl. Phys. Lett.* **92** 041110

[30] Suzuki T, Arai Y, Ohishi Y 2008 Quantum efficiencies of near-infrared emission from Ni^{2+}-doped glass-ceramics *J. Lumin.* **128** 603.

[31] Golubev N V, Savinkov V I, Ignat'eva E S, Lotarev S V, Sarkisov P D, Sigaev V N, Bulatov L I, Mashinskii V M, Plotnichenko V G and Dianov E M 2010 Nickel-doped gallium containing glasses luminescent in the near infrared spectral range *Glass Phys. Chem.* **36** 657

[32] de Mello J C, Wittmann H F and Friend R H 1997 An improved experimental determination of external photoluminescence quantum efficiency *Adv. Mater.* **9** 230–232

[33] Lakowicz J R 1999 *Principles of Fluorescence Spectroscopy* (Kluwer Academic, Plenum: New York) p 367